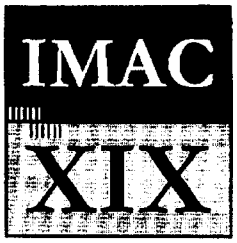

Proceedings

of

IMAC-XIX: A Conference on Structural Dynamics

FEBRUARY 5-8, 2001
HYATT ORLANDO
KISSIMMEE, FLORIDA

The IMAC-XIX Proceedings are dedicated to the memory of Dominick J. DeMichele, IMAC Founder and SEM Honorary Member

TECHNICAL PROGRAM CHAIRS:
Alfred L. Wicks, Virginia Polytechnic Institute and State University
Raj Singhal, David Florida Laboratory of the Canadian Space Agency

SOCIETY FOR EXPERIMENTAL MECHANICS, INC.:
Patricia Deuschle, Acting Executive Director
Katherine M. Ramsay, Conference Manager

Organized By:

SOCIETY FOR EXPERIMENTAL MECHANICS, INC.
7 School Street, Bethel, Connecticut 06801

Buffet Alleviation of Twin-Tailed Fighter Aircraft Using Saturation-Based Control

Ayman A. El-Badawy and **Ali H. Nayfeh**

A.O. Smith Electrical Products Company
Department of Engineering Science and Mechanics
Virginia Polytechnic Institute and State University
Blacksburg, VA 24061, USA

ABSTRACT

We investigated the use of saturation-based control to suppress high-amplitude vibrations of a structural dynamic model of a twin-tail assembly of the F-15 fighter when subjected to a primary resonance excitation. We developed the nonlinear differential equations of motion and obtained an approximate solution using the method of multiple scales. Then, we conducted bifurcation analyses for the open- and closed-loop response of the system and investigated theoretically the performance of the control strategy. The theoretical findings indicate that the control law leads to effective vibration suppression and bifurcation control. We conducted experiments to verify the theoretical analysis. We built a digital control system that consists of the SIMULINK modeling software and a dSPACE DS1103 controller installed in a personal computer, and we used actuators made of piezoelectric ceramic material. The experimental results show that saturation-based control is effective in suppressing steady-state vibrations.

NOMENCLATURE

t	time
$u_i(t)$	generalized coordinates
ω_i	natural frequencies
Ω	driving frequency
σ_i	detunings that describe the nearness of Ω to ω_i
α_i	coefficients of the cubic nonlinearity of the tails
μ_i	viscous damping coefficients of the tails
μ_3, μ_4	aerodynamic damping coefficients of the tails
k	coupling coefficient of the twin tails
τ_i	arbitrary phase angles
u_{ij}	terms in the expansion of u(t)
F	amplitude of the excitation force
ϵ	small bookkeeping parameter
ζ_3, ζ_4	linear damping coeffecients of the filters
ρ_i	feedback gains
p_i, q_i	coefficients in the frequency response equation

1 INTRODUCTION

Buffeting is defined as the response of aircraft structures (such as wings and tails) to unsteady flow [1]. A typical fighter aircraft, such as the F-15, performs maneuvers at high angles of attack. Depending on the angle of attack and the freestream velocity, vortical flows impinge on the tails and create large dynamic responses, which result in large dynamic loads and stresses throughout the tail structure. These loads may excite different vibration modes that cause severe structural fatigue damage and premature failure. Thus it is important to reduce the unwanted vibrations caused by buffet loads and thus extend the fatigue life of the F-15 vertical tails.

The idea behind saturation-based control is that in weakly nonlinear systems, internal resonances may occur if the linear natural frequencies are commensurate or nearly commensurate, and internal resonances provide coupling and energy exchange among the vibration modes. If two natural frequencies of a system with quadratic nonlinearities are in the ratio 2:1, there exists a saturation phenomenon [2]. When the system is excited at a frequency near the higher natural frequency, the structure responds at the frequency of excitation and the amplitude of the respoonse increases linearly with the amplitude of excitation. However, when the high-frequency modal amplitude reaches a critical value, this mode saturates and all additional energy added to the system by increasing the excitation amplitude overflows into the low-frequency mode. The critical amplitude at which the energy transfers to the low-frequency mode depends on the damping in the low-frequency mode and the detuning between the encounter frequency and twice the natural frequency of the low-frequency mode. The smaller these two quantities are, the smaller the critical amplitude is.

The technique is similar to that of the positive position feedback control developed by Fanson and Caughey [3] in that a tuned second-order compensator circuit is used to suppress oscillatory motion , but nonlinear coupling is used instead of coupling the controller to the system linearly. Thus make use of the ability

to transfer energy using the mechanism of internal resonance in nonlinear systems.

2 THEORETICAL DEVELOPMENT

The closed-loop response of the twin tails to a primary resonance excitation can be modeled by two mass-normalized second-order coupled differential equations, while the dynamics of the two filters can be modeled by two second-order differential equations. The first filter targets the response of the right tail, while the second filter targets the response of the left tail. The governing equations can be written as

$$\ddot{u}_1 + \omega_1^2 u_1 + 2\epsilon\mu_1\dot{u}_1 + \epsilon\alpha_1 u_1^3 + \epsilon\mu_3\dot{u}_1 \mid \dot{u}_1 \mid - \epsilon k(u_2 - u_1) = \epsilon F\cos(\Omega t + \tau_1) + \epsilon\rho_1 u_3^2 \quad (1)$$

$$\ddot{u}_2 + \omega_2^2 u_2 + 2\epsilon\mu_2\dot{u}_2 + \epsilon\alpha_2 u_2^3 + \epsilon\mu_4\dot{u}_2 \mid \dot{u}_2 \mid - \epsilon k(u_1 - u_2) = \epsilon F\cos(\Omega t + \tau_2) + \epsilon\rho_2 u_4^2 \quad (2)$$

$$\ddot{u}_3 + \omega_3^2 u_3 + 2\epsilon\zeta_3\dot{u}_3 = \epsilon\rho_3 u_1 u_3 \quad (3)$$

$$\ddot{u}_4 + \omega_4^2 u_4 + 2\epsilon\zeta_4\dot{u}_4 = \epsilon\rho_4 u_2 u_4 \quad (4)$$

where u_1 and u_2 denote the generalized coordinates of the first bending modes of the twin-tail assembly, u_3 and u_4 denote the filters coordinates, ω_1 and ω_2 are the lowest linear natural frequencies of the right and left tails, ω_3 and ω_4 are the frequencies of the filters, μ_1, μ_2, ζ_3, and ζ_4 are the linear damping coeffecients, α_1 and α_2 are the coeffecients of the cubic nonlinearity, μ_3 and μ_4 are aerodynamic damping coefficients, k is the coupling coefficient of the twin tails, and $F\cos(\Omega t+\tau_1)$, $\rho_1, \cdots, \rho_4$ are feedback gains and $F\cos(\Omega t+\tau_2)$ are the direct excitations of the tail section. Here, ϵ is a bookkeeping parameter, which can be set equal to unity in the final analysis. The parameters in equations (1)-(4) were identified using experimental data [4]. They are listed in Appendix I.

We use the method of multiple scales [5] to generate a first-order approximate solution of equations (1)–(4) when $\Omega \approx \omega_1$, $\omega_2 \approx \omega_1$, $\omega_3 \approx \omega_1$ and $\omega_4 \approx \omega_2$.

3 PERFORMANCE OF THE CONTROL LAW

Using the method of multiple scales [5], we determined the equations governing the modulation of the amplitudes and phases of the modes. The result is

$$p_1' = -\mu_1 p_1 + \frac{1}{2\omega_1}\eta_1 k q_1 - \nu_1 q_1 + \frac{3}{8\omega_1}\alpha_1 p_1^2 q_1 + \frac{3}{8\omega_1}\alpha_1 q_1^3 - \frac{1}{2\omega_1}\eta_1 k q_2 - \frac{4}{3\pi}\mu_3\omega_1\sqrt{p_1^2+q_1^2}\,p_1 - \frac{\rho_1}{2\omega_1}p_3 q_3 \quad (5)$$

$$q_1' = \frac{1}{2\omega_1}F - \frac{1}{2\omega_1}\eta_1 k p_1 + \nu_1 p_1 - \frac{3}{8\omega_1}\alpha_1 p_1^3 + \frac{1}{2\omega_1}\eta_1 k p_2 - \mu_1 q_1 - \frac{4}{3\pi}\mu_3\omega_1\sqrt{p_1^2+q_1^2}\,q_1 - \frac{3}{8\omega_1}\alpha_1 p_1 q_1^2 + \frac{\rho_1}{4\omega_1}p_3^2 - \frac{\rho_1}{4\omega_1}q_3^2 \quad (6)$$

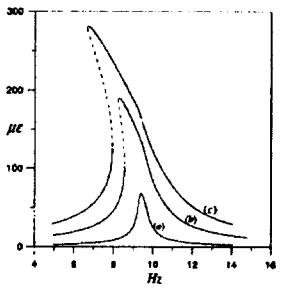

(i) right-tail response

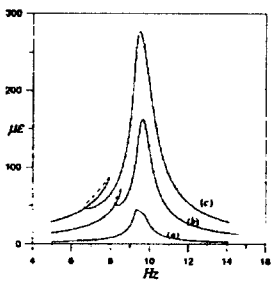

(ii) left-tail response

Figure 1: Effect of varying the excitation amplitude on the frequency-response curves of the two tails: a) F=0.33g, b) F=1.65g, and c) F=3.3g.

$$p_2' = -\mu_2 p_2 + \frac{1}{2\omega_1}\eta_2 k q_1 - 4k\eta_2 q_2 - \nu_2 q_2 + \frac{3}{8\omega_2}\alpha_2 p_2^2 q_2 + \frac{3}{8\omega_2}\alpha_2 q_2^3 - \frac{4}{3\pi}\mu_3\omega_1\sqrt{p_1^2+q_1^2}\,p_1 - \frac{\rho_2}{2\omega_2}p_4 q_4 \quad (7)$$

$$q_2' = \frac{1}{2\omega_2}F + \frac{1}{2\omega_2}\eta_2 k p_1 - \frac{1}{2\omega_2}\eta_2 k p_2 + \nu_2 p_2 - \frac{3}{8\omega_2}\alpha_2 p_2^3 - \mu_2 q_2 - \frac{4}{3\pi}\mu_4\omega_2\sqrt{p_2^2+q_2^2}\,q_2 - \frac{3}{8\omega_2}\alpha_2 p_2 q_2^2 + \frac{\rho_2}{4\omega_2}p_4^2 - \frac{\rho_2}{4\omega_2}q_4^2 \quad (8)$$

$$p_3' = -\zeta_3 p_3 - \frac{\rho_3}{4\omega_3}p_3 q_1 - \nu_3 q_3 + \frac{\rho_3}{4\omega_3}p_1 q_3 \quad (9)$$

$$q_3' = \nu_3 p_3 + \frac{\rho_3}{4\omega_3}p_1 p_3 - \zeta_3 q_3 + \frac{\rho_3}{4\omega_3}q_1 q_3 \quad (10)$$

$$p_4' = -\zeta_4 p_4 - \frac{\rho_4}{4\omega_4}p_4 q_2 - \nu_4 q_4 + \frac{\rho_4}{4\omega_4}p_2 q_4 \quad (11)$$

$$q_4' = \nu_4 p_4 + \frac{\rho_4}{4\omega_4}p_2 p_4 - \zeta_4 q_4 + \frac{\rho_4}{4\omega_4}q_2 q_4 \quad (12)$$

The performance of the control was evaluated by calculating the equilibrium solutions of equations (5)–(12) and examining their stability as a function of the frequency of excitation and the gains ρ_i. Thus, we set the time derivatives in equations (5)–(12) equal to zero and solved the resulting system of algebraic equations for the p_i and q_i for a specified value of one of the

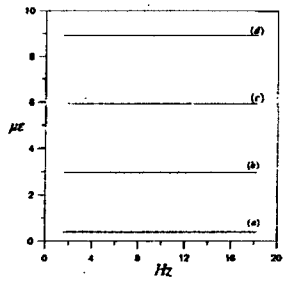

(i) right tail

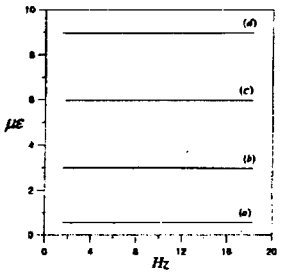

(ii) left tail

Figure 2: Effect of varying the damping ratios of the two absorbers on the frequency-response curves of the two tails (F=3.3g, $G_i = 1$): a) $\zeta_{3,4}$=0.01, b) $\zeta_{3,4}$=0.1, c) $\zeta_{3,4}$=0.2, and d) $\zeta_{3,4}$=0.3.

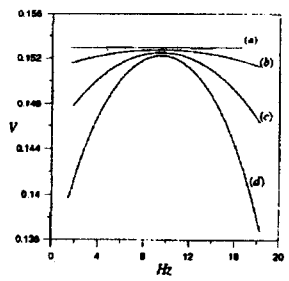

(i) right tail

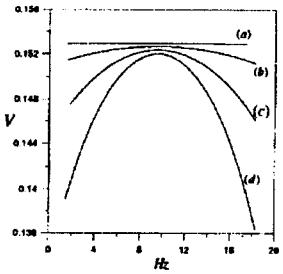

(ii) left tail

Figure 3: Effect of varying the damping ratios of the two absorbers on their frequency-response curves (F=3.3 g, $G_i = 1$): a) $\zeta_{3,4}$=0.01, b) $\zeta_{3,4}$=0.1, c) $\zeta_{3,4}$=0.2, and d) $\zeta_{3,4}$=0.3.

parameters. The amplitudes a_1, a_2, a_3, and a_4 of the responses of the two tails and the two filters were then calculated from $a_i = \sqrt{p_i^2 + q_i^2}$. Since there is no closed-form solution for the eight algebraic equations, we resorted to numerical techniques. Numerical integration of the modulation equations for different sets of initial conditions was used to locate some of the possible solutions for a given frequency and amplitude of excitation. Then, starting with these solutions, we used a pseudo-arclength scheme [6] to trace the branches of the equilibrium solutions by varying the excitation frequency.

The stability of a particular equilibrium solution was determined by examining the eigenvalues of the Jacobian matrix of the right-hand sides of equations (5)–(12). If the real part of every eigenvalue is negative, the corresponding equilibrium solution is asymptotically stable. If the real part of any of the eigenvalues is positive, the corresponding equilibrium solution is unstable. In the next two sections, we present the stability analysis and evaluation of the control law.

In Figure 1, we show frequency-response curves for the open-loop case for various levels of the excitation amplitude. The amplitude of the response depends on the detuning and amplitude of the excitation. Solid lines correspond to stable solutions, while dashed lines correspond to unstable solutions. All of the bifurcations are saddle-node bifurcations. For the right tail, it is clear that, as the amplitude of excitation increases, the frequency-response curves bend away from the linear curves, resulting in multivalued regions. The multivaluedness is responsible for jumps. The left tail has multivalued responses in the region between 6-8 Hz. We note here that, as the forcing amplitude increases, the nonlinearity will dominate the response. In fact, twin-tail aircraft are often subjected to high-intensity buffet loads that produce accelerations in excess of $450g$ at the tip of the vertical tail during maneuvers at high angles of attacks[8]. In the next two sections, we assume that the excitation amplitude is $3.3g$, (i.e., we operate on curve (c) in figure 1).

4 THEORETICAL FREQUENCY-RESPONSE CURVES

Figures 2 and 3 show frequency-response curves of the two tails and the two absorbers. The frequencies of the absorbers were automatically tuned one-half the excitation frequency. To the-

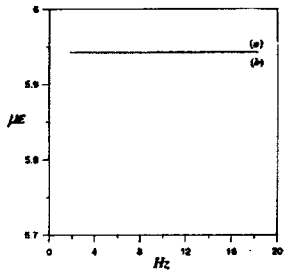

(i) right tail

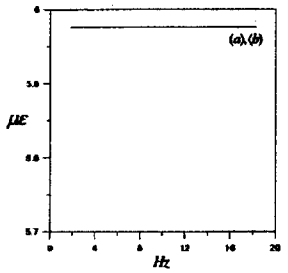

(ii) left tail

Figure 4: Effect of varying the feedback gain on the frequency-response curves of the two tails when their frequencies are fixed ($\zeta_{3,4}$=0.2, F=3.3g): a) G=1 and b) G=0.5.

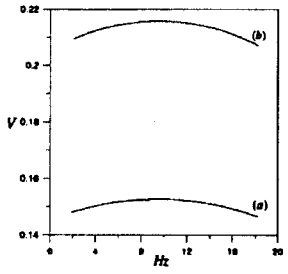

(i) right tail

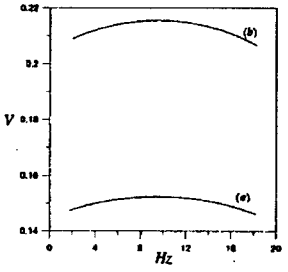

(ii) left tail

Figure 5: Effect of varying the feedback gain on the frequency-response curves of the two absorbers when their frequencies are fixed ($\zeta_{3,4}$=0.2, F=3.3g): a) G=1 and b) G=0.5.

oretically implement this, for example for the right tail, we set $\Omega = \omega_1 + \sigma_1$ and $2\omega_3 = \omega_1 - \sigma_3$, where Ω is the excitation frequency, ω_1 is the natural frequency of the right tail, and ω_3 is the frequency of the absorber. The latter is tuned to the response frequency of the first mode of the right tail. If we set $\sigma_3 = \sigma_1$ (i.e., twice the absorber frequency is equal to the excitation frequency) during a frequency sweep, we obtain Figure 2(i). A similar analysis was done for the left tail (Figure 2(ii)). We note that σ_2 is fixed to be to $\omega_2 - \omega_1 = 0.085$Hz.

Figures 4 and 5 show the effect of varying the feedback gain on the responses of the tails and the absorbers. These figures were obtained while tuning the frequencies of the absorbers to be equal to one-half the excitation frequency (i.e., $\omega_3 = \omega_4 = \frac{1}{2}\Omega$) and a damping ratio $\zeta_{3,4} = 0.2$. As the gain was increased, the responses of the tails and the absorbers decreased. However, since the control force was generated by the tail vibration itself, the controller vibration amplitude can never approach zero.

Figures 6 and 7 show the effect of detuning the absorbers' frequency away from one-half the excitation frequency. As can be seen, the response of the tails degrade when $\omega_{abs} = \frac{1}{2}\Omega - 2$. We also expect the behavior to keep degrading the more the detuning is. Thus the implementation of the technique is rendered very effective by tuning the frequency of the absorber equal to the frequency of oscillation of the tail.

5 THEORETICAL FORCE-RESPONSE CURVES

In Figures 8 and 9, we show the closed-loop force-response curves of the two tails and the two absorbers. These figures illustrate the well-known saturation phenomenon. Where the response of the directly excited mode does not vary with the excitation amplitude. In fact, the value of the amplitude is kept fixed. We note that the response amplitude of the tails depend on the damping and the external detuning in the system. Figure 8 is generated for a damping ratio of $\zeta_{3,4}$=0.01 of the quadratic absorbers and perfect tuning (natural frequency of the absorber is set equal to one-half the excitation frequency). In fact, as the damping ratio of the absorbers increase, the response of the tails increase. This can be explained by mentioning that as the damping ratio of the absorbers increase, it takes more forcing of the tails for the energy to channel from the tails to

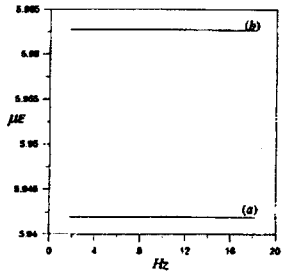

(i) right tail

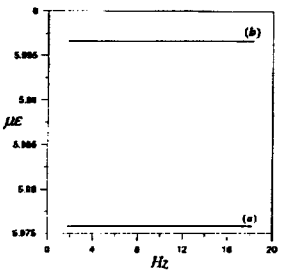

(ii) left tail

Figure 6: Effect of detuning the absorber frequency on the frequency-response curves of the two tails when their frequencies are fixed (F=3.3 g): a) $w_{3,4} = \frac{1}{2}\Omega$ and b) $w_{3,4} = \frac{1}{2}\Omega - 2$

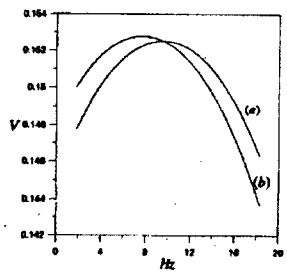

(i) right tail

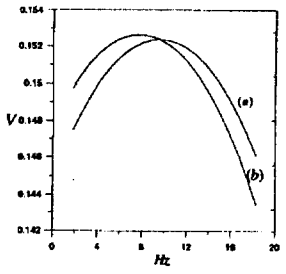

(ii) left tail

Figure 7: Effect of detuning the two absorber frequencies on their frequency-response curves when their frequencies are fixed(F=3.3 g): a) $w_{3,4} = \frac{1}{2}\Omega$, b) $w_{3,4} = \frac{1}{2}\Omega - 2$

the absorbers.

6 EXPERIMENTAL RESULTS

To test the control method, we built a digital control system using the SIMULINK modeling software [7] and a dSPACE controller [8] in a personal computer. The SIMULINK software is used to build the control block diagram, and then the dSPACE real-time workshop is used to generate a C-code from the SIMULINK model. The C-code is then connected by the dSPACE real-time interface to the dSPACE real-time hardware system. Figure 10 shows the experimental setup. The tail deflections were measured with two strain gages. The actuators were two piezoelectric patches made from lead-zirconate-titanate. One patch was placed near the root of each tail. The tails were excited by two other PZT patches placed on the outer sides of the tails. The tail section used in the experiments is a 1/16 dynamically scaled model of the F-15 tail assembly. The model was constructed at the laboratory of Professor Sathya Hanagud at the Georgia Institute of Technology from a series of aluminum channels, brass rings, composite plates, metal masses, and various adhesives. The model is approximately 0.355 m long, 0.228 m tall, and 0.482 m wide.

The maximum tail vibration achieved with the PZT actuators was $0.33V \approx 62\mu\epsilon$, which is in the linear response range of the tails (refer to Figure 1). The conversion follows the following equation

$$\mu\epsilon = \frac{4V_{out}}{10 \times 1000 \times 2.12 \times 10^{-6}} \qquad (13)$$

where 10 is the bridge excitation, 1000 is the amplifier gain, and 2.12 is the gage factor.

Figure 11 show the time histories of the open- and closed-loop responses of the right tail. Similar results were obtained for the left tail. It is clear that the amplitudes of the responses are reduced by almost 10 times.

Figure 12 shows the control signal sent to the power amplifier, which in turn was sent to the PZT actuators. We note that there is a DC offset of the signal due to squaring the coupling term. In fact, this DC term is not desirable from the standpoint of the piezo amplifier.

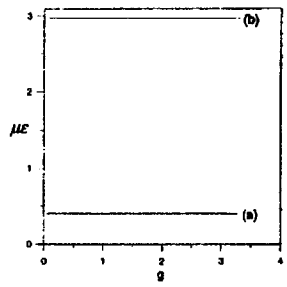

(i) right tail

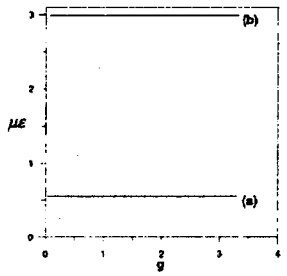

(ii) left tail

Figure 8: Force-response curves of the two tails (freq=9.135 Hz, $\zeta_{3,4}$=0.01)

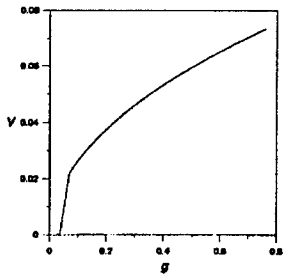

(i) right tail

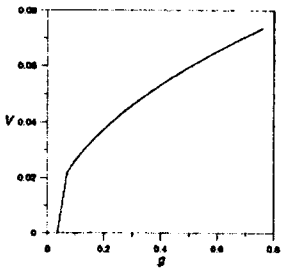

(ii) left tail

Figure 9: Force-response curves of the two absorbers (freq=9.135 Hz, $\zeta_{3,4}$=0.01)

7 CONCLUSION

A saturation-based control law was used to suppress the vibrations of the first bending modes of the twin tails of a 1/16 structural dynamic model of an F-15 twin-tail assembly when subjected to primary excitations. The dynamics of the first flexural modes of the twin tails are modeled by two second-order coupled nonlinear ordinary-differential equations. A filter is coupled linearly to one of the tails. The method of multiple scales is used to derive eight first-order differential equations governing the amplitudes and phases of the response. Then a bifurcation analysis is conducted to examine the stability of the closed loop system and investigate the performance of the control law. The control eliminates all multiple responses. The amplitudes of oscillation of the tails decrease tremendously. Once the absorbers frequencies are properly tuned, we show that the control scheme possesses a wide suppression bandwidth. Also, a parametric investigation was carried out to see the effect of changing the damping ratio of the absorber, the value of the feedback gain and the effect of detuning the frequencies of the absorbers in the response of the tails. To verify the theoretical analysis, experiments are done on the structural model of the twin-tail assembly fitted with piezoceramic actuators. We implement the absorber using a digital signal processing (DSP) device. Good agreement between theory and experiments is found.

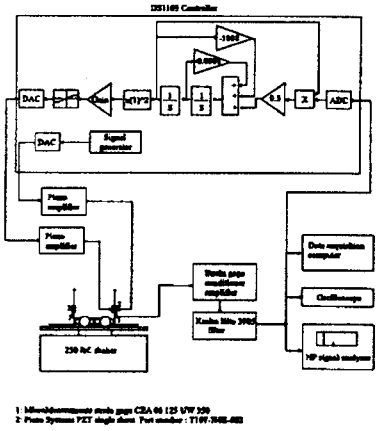

Figure 10: Experimental setup.

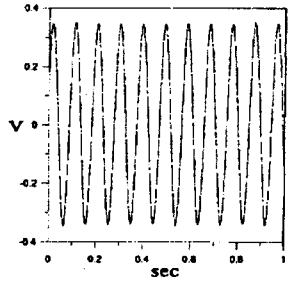

(i) open loop

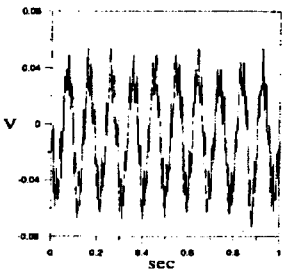

(ii) closed loop

Figure 11: Response of the right tail ($\zeta_{3,4} = 0.1$)

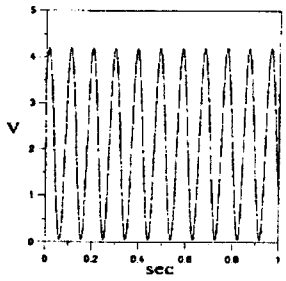

(i) time domain

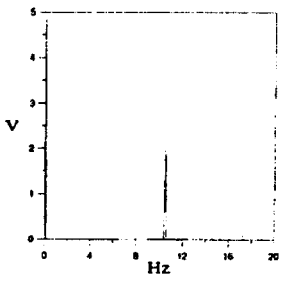

(ii) frequency domain

Figure 12: Control signal.

APPENDIX I

We estimated the parameters of the model from regressive fits of the experimentally and theoretically determined steady-state response amplitudes. The identified parameters for the right tail are $\omega_1 = 9.135Hz$, $\zeta_1 = 0.01357$, $\mu_3 = 3.157 \times 10^{-4}\mu\epsilon^{-1}$, $\alpha_1 = -3.675 \times 10^{-2}\frac{1}{s^2\mu\epsilon^2}$, and $\eta_1 = 161.54\frac{1}{gs^2}$. The identified parameters for the left tail are $\omega_2 = 9.05Hz$, $\zeta_2 = 0.01856$, $\mu_4 = 1.958864 \times 10^{-4}\mu\epsilon^{-1}$, $\alpha_2 = -2.977 \times 10^{-3}\frac{1}{s^2\mu\epsilon^2}$, and $\eta_2 = 275.12\frac{1}{gs^2}$. The estimated value for $k = 87(1/sec^2)$.

ACKNOWLEDGEMENT

This work was supported by the Air Force Office of Scientific Research under Grant No. F496020-98-1-0393.

REFERENCES

[1] **Mabey, D. G.**, *'Some Aspects of Aircraft Dynamic Loads Due To Flow Separation', Progress in Aerospace Science'*, vol.26, pp. 115–151, 1989.

[2] **Nayfeh, A. H.**, and **Mook, D. T.**, Nonlinear Oscillations, Wiley-Interscience, New York, 1979.

[3] **Fanson, J. L., & Caughey, T. K.**, *'Positive Position Feedback Control for Large Space Structures'*, AIAA Journal, vol.28 , pp. 717–724, 1990.

[4] **El-Badawy, A. A.**, and **Nayfeh, A.H.** *'Nonlinear Identification of a Scaled Structural Dynamic Model of the F-15 Tail Section'*, 17th International Modal Analysis Conference, Kissimmee, Fl, pp. 1175–1181, 1999.

[5] **Nayfeh, A. H.**, Introduction to Perturbation Techniques, Wiley-Interscience, New York, 1981.

[6] **Nayfeh, A. H.**, and **Balachandran, B.**, Applied Nonlinear Dynamics, Wiley-Interscience, New York, 1995.

[7] *'SIMULINK: Dynamic System Simulation Software.'* Natick, MA: The MathWorks.

[8] *'dSPACE digital signal processing and control engineering.'* GmbH, Paderborn, Germany.